An Efficient Algorithm to Determine the Operational Range of Near-Field On-Body UHF RFID Systems

Alessandro Felaco, Kamil Yavuz Kapusuz, Hendrik Rogier, Dries Vande Ginste

Department of Information Technology, IDLab, Ghent University/IMEC, Belgium

{Alessandro.Felaco, KamilYavuz.Kapusuz, Hendrik.Rogier, Dries.VandeGinste}@UGent.be

Abstract — A new algorithm is proposed, leveraging a 3D multipole expansions of the electromagnetic fields, to accurately determine the operational range of a radiative near-field on-body radio-frequency identification (RFID) system based on its far field radiation patterns, simulated or measured, under realistic deployment conditions. We illustrate the advocated method by an interrogating 866 MHz standard gain horn (SGH) and a passive eighth-mode substrate integrated waveguide (SIW) textile antenna deployed on an arm. The resulting algorithm is order 10^7 times faster than full-wave software, largely outperforms the range calculation via the traditional far field link method and it is capable of very accurately predicting the exchanged power.

Keywords — Body area network (BAN), far field, near-field, radio-frequency identification (RFID), spherical modes expansion.

I. INTRODUCTION

The Internet-of-Things (IoT) paradigm envisions to employ off-body, on-body or even in-body [1]–[7] ultra-high frequency (UHF) radio-frequency identification (RFID) devices allowing smart-systems to self-operate, improving efficiency and productivity. While an antenna-rich environment is potentially favorable for many interesting applications, at the same time designers have to deal with the trade-off between system performance, in terms of RFID range [8], [9], and electromagnetic pollution.

For near-field RFID design, the most direct approach is that of resorting to a far field system that operates at the maximum allowed effective isotropic radiated power (EIRP) [10]. This leads to a waste of energy and it makes it harder to comply with specific absorption rate (SAR) regulations [11]. Moreover, this approach ignores essential near-field interactions [12], which results in malfunctions or detection of unrelated devices [13], [14]. Alternatively, to optimize dedicated near-field RFID systems, designers can opt for full-wave software [15]–[17] or small- and large-scale fading models [18]. However, these are either too computationally expensive or provide only strictly environment-specific solutions that require accurate preemptive measurements. Hence, there is need for an efficient, yet still accurate tool to study the radiative near-field behavior of RFID systems.

In this contribution, we propose a novel far-to-near-field transformation, based on a multipole expansion of the RFID system's far fields. In contrast to [19], where the advocated algorithm is applied to a RFID tag antenna on the chest, here we focus on the more challenging case of deployment on the arm. The far fields are measured or simulated when deploying the RFID tag on-body, as such accounting for platform effects.
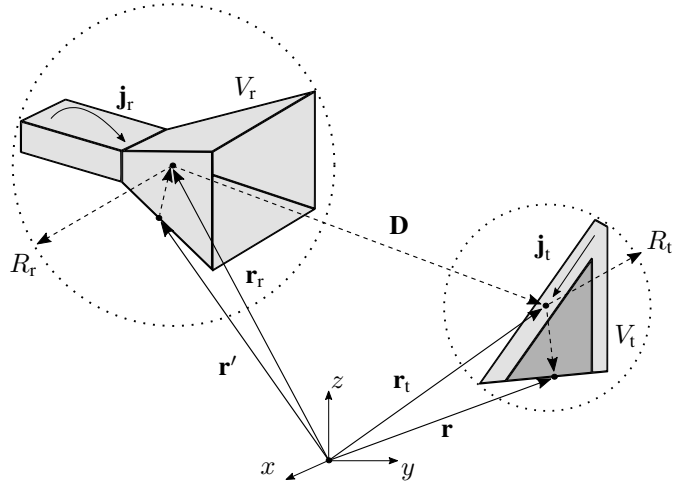

Fig. 1. RFID system composed of reader and tag represented by current densities $\mathbf{j}_r$ and $\mathbf{j}_t$, present in volumes V_r and V_t located at $\mathbf{r}_r$ and $\mathbf{r}_t$ and circumscribed by spheres of radius R_r and R_t, respectively (for a detailed description, see [19]).

The proposed algorithm precomputes the interactions between transmitting and receiving multipoles in closed form, and then stores them within highly sparse structures. The bulk of the computation is reduced to matrix-to-vector products between the interaction matrices and the far fields' expansion coefficients, yielding extremely fast and efficient results. Moreover, this method is unaffected by the simulation volume and frequency, it requires but a tiny fraction of the memory and computational time required by full-wave software and it is massively more accurate than the straightforward far field approximation of near-field systems.

II. THEORY

Consider the RFID system of Fig. 1. The open-circuit voltage V_o induced on the tag antenna by the reader is determined by the reciprocity theorem to be [20]

$$V_o = -Z_{a,t} \int_{V_t} \mathbf{E}_r(\mathbf{r}) \cdot \mathbf{j}_{t,V}(\mathbf{r}) \, d\mathbf{r}, \tag{1}$$

where $Z_{a,t}$ is the tag's input impedance, $\mathbf{E}_r$ is the electric field generated by the reader and $\mathbf{j}_{t,V}$ is the voltage-normalized current density obtained when exciting the tag in transmit mode. If the antennas are spaced far enough so that their reactive near-fields do not couple, then $\mathbf{E}_r$ is given by [21]

$$\mathbf{E}_r(\mathbf{r}) = -j\omega\mu \int_{V_r} \boldsymbol{\mathcal{G}}(\mathbf{r}, \mathbf{r}') \cdot \mathbf{j}_r(\mathbf{r}') \, d\mathbf{r}', \tag{2}$$

where ω is the angular velocity, μ is the free-space permeability, $\mathcal{G}$ is the 3-D dyadic Green function and where we limit the integration domain to V_r. For non-overlapping circumscribing spheres, we combine the spherical Hankel functions' addition theorem [22] with the plane waves expansion [23, p. 410] to express $\mathcal{G}$ as

$$\mathcal{G}(\mathbf{r}, \mathbf{r}') = -\frac{jk}{4\pi} \sum_{l,m}^{\infty} \mathcal{H}_l^m(k\mathbf{D}) \oiint_\Omega \left[\mathcal{I} - \hat{\mathbf{k}}\hat{\mathbf{k}} \right] e^{-j\mathbf{k}\cdot\mathbf{d}} \bar{Y}_l^m(\hat{\mathbf{k}}) \, d\hat{\mathbf{k}}, \tag{3}$$

where k is the wave number, $\mathcal{I}$ is the unit dyadic and $(\mathbf{r} - \mathbf{r}') = (\mathbf{D} + \mathbf{d})$, with $\mathbf{D} = (\mathbf{r}_t - \mathbf{r}_r)$, $\mathbf{d} = (\mathbf{r}_r - \mathbf{r}') + (\mathbf{r} - \mathbf{r}_t)$. The hat symbol indicates a unit vector. Further, the spherical function $\mathcal{H}_l^m$ is defined by

$$\mathcal{H}_l^m(k\mathbf{D}) = j^{-l} h_l^{(2)}(kD) Y_l^m(\hat{\mathbf{D}}), \tag{4}$$

where $h_l^{(2)}$ is a spherical Hankel function of the second kind and Y_l^m is a scalar spherical harmonic [24].

Combining (1), (2) and (3) with the following definition of the far field radiation vector

$$\mathbf{F}(\hat{\mathbf{k}}) = -\frac{j\omega\mu}{4\pi} \int_V e^{j\mathbf{k}\cdot(\mathbf{r}'-\mathbf{r})} \left[\mathcal{I} - \hat{\mathbf{k}}\hat{\mathbf{k}} \right] \cdot \mathbf{j}(\mathbf{r}') \, d\mathbf{r}', \tag{5}$$

we express the open-circuit voltage induced on the tag as

$$V_o = -\frac{4\pi}{\eta_0} Z_{a,t} V_{a,r} \sum_{l,m}^{L} c_l^m \mathcal{H}_l^m(k\mathbf{D}), \tag{6}$$

where η_0 is the free-space impedance and $V_{a,r}$ represents the voltage present at the reader's port. To exclude highly attenuated higher-order harmonic modes from the computation [25], the summation in (6) is truncated at $L = \min(L_r, L_t)$, where [26]

$$L_r = kR_r + 6\sqrt[3]{kR_r}, \tag{7}$$

$$L_t = kR_t + 6\sqrt[3]{kR_t}. \tag{8}$$

The expansion coefficients c_l^m in (6) arise from the interactions between reader's and tag's voltage-normalized far field radiation patterns $\mathbf{F}_{r,V}$ and $\mathbf{F}_{t,V}$, respectively, and are defined by

$$c_l^m = \mathbf{e}_r^\dagger \left[\mathbf{C}_l^m \mathbf{m}_t - \mathbf{S}_l^m \mathbf{e}_t \right] + \mathbf{m}_r^\dagger \left[\mathbf{S}_l^m \mathbf{m}_t - \mathbf{C}_l^m \mathbf{e}_t \right], \tag{9}$$

where $\dagger$ indicates conjugate transpose. The $(\mathbf{e}_r, \mathbf{m}_r)$ and $(\mathbf{e}_t, \mathbf{m}_t)$ store the reader's and tag's coefficients stemming from the following spherical harmonic decomposition,

$$\mathbf{F}_V = \sum_{l,m}^{L} e_l^m \boldsymbol{\mathcal{E}}_l^m + m_l^m \boldsymbol{\mathcal{M}}_l^m. \tag{10}$$

These coefficients are thus defined for each device by

$$e_l^m = \oiint_\Omega \langle \mathbf{F}_V, \boldsymbol{\mathcal{E}}_l^m \rangle \, d\hat{\mathbf{k}}, \tag{11}$$

$$m_l^m = \oiint_\Omega \langle \mathbf{F}_V, \boldsymbol{\mathcal{M}}_l^m \rangle \, d\hat{\mathbf{k}}, \tag{12}$$

where the angle brackets indicate an Hermitian inner product [27] and the symbols $\boldsymbol{\mathcal{E}}_l^m$ and $\boldsymbol{\mathcal{M}}_l^m$ denote two sets
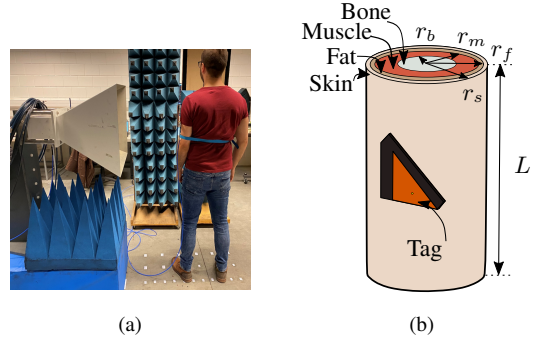

(a)   (b)

Fig. 2. (a) The tag antenna was strapped on an arm and the received signal was measured in the positions indicated by the ground markers, placed between λ to 3λ in length and $-\lambda$ to λ in width. (b) Equivalent virtual model of the deployed tag. Dimensions are $L = 300$ mm, $r_s = 50$ mm, $r_f = 49$ mm, $r_m = 46$ mm, $r_b = 10$ mm. Tissue parameters at 868 GHz: (1) skin, $\epsilon_r = 41.6$, $\sigma = 0.87$ S/m, (2) fat, $\epsilon_r = 5.46$, $\sigma = 0.051$ S/m, (3) muscle, $\epsilon_r = 55.1$, $\sigma = 0.93$ S/m, (4) bone, $\epsilon_r = 12.45$, $\sigma = 0.14$ S/m.

of orthonormal transversal vector spherical harmonics [28, eq. (19, 38)] expressed as a linear combination of spin-1 tensor spherical harmonics [29, eq. (3)]. The $\mathbf{S}_l^m$ and $\mathbf{C}_l^m$ matrices in (9) collect the interactions between the reader's and tag's multipoles, expressed as a combination of Clebsch-Gordan coefficients. Owing to their properties [30, eq. (27.9.2–27.9.9)], these matrices exhibit a sparsity higher than 95%. They only need to be computed once and are very efficient to store. Thus, they can be reused for any other experiment, resulting in extremely effective simulations.

III. VALIDATION

A. Validation via Measurements

A 866 MHz NSI-RF-SG975 standard gain horn (SGH) [31] with gain of $G_r = 13$ dBi, input power of $P_{a,r} = -15$ dBm and EIRP = -2 dBm was employed as interrogating device to validate the advocated method. The choice of tag fell on a passive eighth-mode substrate integrated waveguide (SIW) antenna [32] loaded with a 50 Ω impedance. It was strapped on an arm and moved in a horizontal plane between λ to 3λ in length and $-\lambda$ to λ in width, as shown in Fig. 2a. A network analyzer measures the system's S-parameters at each position to determine the power received by the tag's load (P_t) as [33]

$$P_t = P_{a,r} \frac{(1 - |\Gamma_t|^2)|S_{21}|^2}{(1 - |\Gamma_{a,r}|^2)|1 - S_{22}\Gamma_t|^2}, \tag{13}$$

where $\Gamma_{a,r}$ and Γ_t are the reflection coefficients at the reader's port and at the tag's load, respectively. To calculate the returned signal strength indicator ($RSSI$), or in other words the fraction of power returned to the reader, the power available in input at the tag's port is determined from P_t and (13) is then applied to the uplink to compute the reverse operating gain.

Subsequently, the reader's and tag's far field radiation patterns were simulated in *CST Microwave Studio 2019* [34] and used as inputs for a *MATLAB R2019a* [35] script implementing the novel algorithm. To take body effects produced by its different tissues into account, the tag's radiation pattern was simulated when deployed on a virtual arm model (Fig. 2b) [36]. Comparisons between numerical calculations, full wave
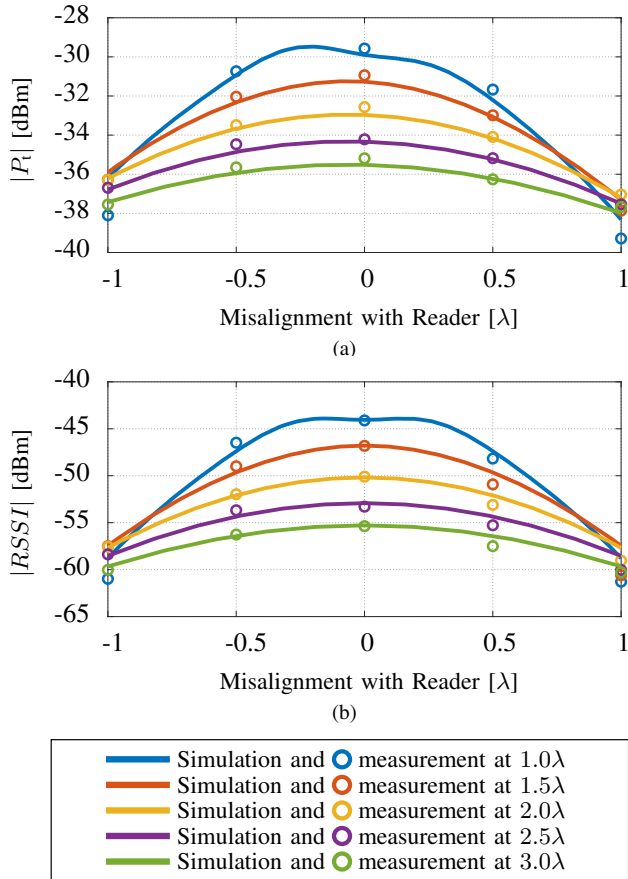
Fig. 3. Measurements and simulations of (a) power received by the tag's load and (b) returned to the reader for the antenna strapped on the arm and moving parallel to the horn's aperture at different distances.
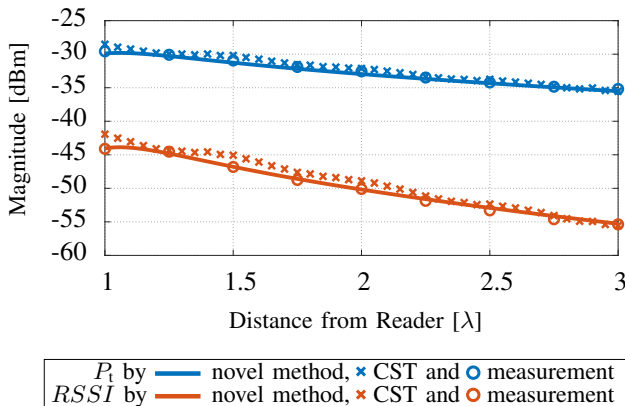

Fig. 4. Measurements and simulations of the power received by the tag's load and returned to the reader when the tag is aligned with the horn's phase center and moved at difference distances.

simulations and measurements are shown in Fig. 3a, 3b and 4, demonstrating an excellent agreement.

To obtain these results, the script required only 30 µs per data point, 70 MB of memory and 2 MB of precomputed values. On the other hand, reproducing the same experiment with the Frequency Domain Solver of *CST Microwave Studio 2019* required 5 minutes per data point and a peak memory usage of 15 GB. Even though the proposed method does not
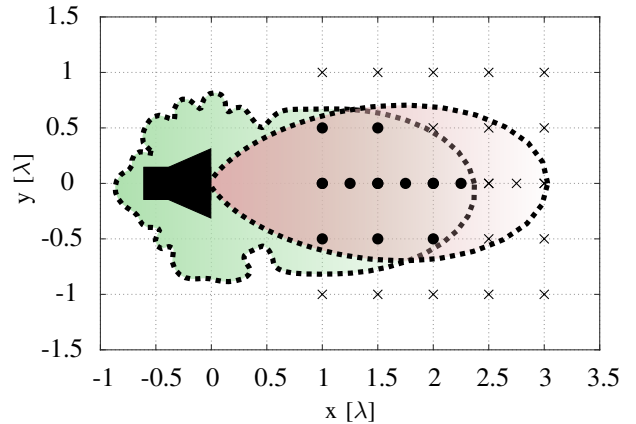

Fig. 5. Operational range of the RFID system obtained through the novel method (green) and the traditional radar approach (red) assuming an activation threshold of P_{th} = -34 dBm. The symbols in the grid show when the tag is turned on (•) or off (×) during the experimental verification.

possess the same generality of full-wave software, it is clearly very valuable for studying the link between RFID devices.

B. Application

To show the superiority of the advocated method over the traditional far field approximation, we compared the predicted operational range in the horizontal plane, containing the phase centers of reader and tag, determined by the novel algorithm and by the traditional radar approach. To numerically verify whether the tag would be turned on at a certain distance, we assumed an activation threshold of P_{th} = -34 dBm and compared the predictions with direct field measurements.

As expected, the operational region obtained through the traditional approach, as seen in Fig. 5, possesses an unrealistic single-lobe profile which, depending on the angle, under- or overestimates the real range by up to λ. On the other hand, the novel algorithm finds a more realistic solution and predicts the correct behavior of the RFID system for all performed experiments.

IV. CONCLUSION

In this contribution, a novel algorithm is presented to efficiently determine the operational range of on-body RFID systems. The method requires a single simulation or measurement of the far field radiation patterns of the RFID devices. As long as there is no interaction through the reactive near-fields, the proposed algorithm is more accurate than the traditional radar equation and faster than full-wave simulations by making use of tensor spherical harmonics decomposition.

REFERENCES

[1] M. A. S. Tajin, C. E. Amanatides, G. Dion, and K. R. Dandekar, "Passive UHF RFID-based knitted wearable compression sensor," *IEEE Internet Things J.*, vol. 8, no. 17, pp. 13 763–13 773, Sep. 2021.

[2] C. Occhiuzzi, S. Cippitelli, and G. Marrocco, "Modeling, design and experimentation of wearable RFID sensor tag," *IEEE Trans. Antennas Propag.*, vol. 58, no. 8, pp. 2490–2498, Aug. 2010.

[3] R. K. Singh, A. Michel, P. Nepa, A. Salvatore, M. Terraroli, and P. Perego, "Compact and wearable yagi-like textile antennas for near-field UHF-RFID readers," *IEEE Trans. Antennas Propag.*, vol. 69, no. 3, pp. 1324–1333, Mar. 2021.

[4] S. Amendola, S. Milici, and G. Marrocco, "Performance of epidermal RFID dual-loop tag and on-skin retuning," *IEEE Trans. Antennas Propag.*, vol. 63, no. 8, pp. 3672–3680, Aug. 2015.

[5] S. Amendola and G. Marrocco, "Optimal performance of epidermal antennas for UHF radio frequency identification and sensing," *IEEE Trans. Antennas Propag.*, vol. 65, no. 2, pp. 473–481, Feb. 2017.

[6] E. Moradi, S. Amendola, T. Bjorninen, L. Sydanheimo, J. M. Carmena, J. M. Rabaey, and L. Ukkonen, "Backscattering neural tags for wireless brain-machine interface systems," *IEEE Trans. Antennas Propag.*, vol. 63, no. 2, pp. 719–726, Feb. 2015.

[7] L. Song and Y. Rahmat-Samii, "An end-to-end implanted brain–machine interface antenna system performance characterizations and development," *IEEE Trans. Antennas Propag.*, vol. 65, no. 7, pp. 3399–3408, Jul. 2017.

[8] P. V. Nikitin and K. V. S. Rao, "Antennas and propagation in UHF RFID systems," in *2008 IEEE Int. Conf. RFID*, Las Vegas, NV, USA, Apr. 2008, pp. 277–288.

[9] L. Sydanheimo, J. Nummela, L. Ukkonen, J. McVay, A. Hoorfar, and M. Kivikoski, "Characterization of passive UHF RFID tag performance," *IEEE Antennas Propag. Mag.*, vol. 50, no. 3, pp. 207–212, Jun. 2008.

[10] P. Nikitin, K. Rao, and S. Lazar, "An overview of near field UHF RFID," in *2007 IEEE Int. Conf. RFID*, Grapevine, TX, USA, Mar. 2007, pp. 167–174.

[11] C. A. Repec, "Regulatory status for using RFID in the EPC gen2 (860 to 960 MHz) band of the UHF spectrum," *GS1: Brussel, Belgium*, 2019.

[12] F. Fuschini, C. Piersanti, L. Sydanheimo, L. Ukkonen, and G. Falciasecca, "Electromagnetic analyses of near field UHF RFID systems," *IEEE Trans. Antennas Propag.*, vol. 58, no. 5, pp. 1759–1770, May 2010.

[13] J. C. Bolomey, S. Capdevila, L. Jofre, and J. Romeu, "Electromagnetic modeling of RFID-modulated scattering mechanism. Application to tag performance evaluation," *Proc. IEEE*, vol. 98, no. 9, pp. 1555–1569, Sep. 2010.

[14] S. Hodges, A. Thorne, H. Mallinson, and C. Floerkemeier, "Assessing and optimizing the range of UHF RFID to enable real-world pervasive computing applications," in *Pervasive Comput.* Springer Berlin Heidelberg, 2007, vol. 4480, pp. 280–297.

[15] U. Khan, S. N. Makarov, Y. Ye, R. Fu, P. Swar, and K. Pahlavan, "Review of computational techniques for performance evaluation of RF localization inside the human body," *IEEE Rev. Biomed. Eng.*, vol. 12, pp. 123–137, 2019.

[16] Y. Futagi, T. Hori, K. Honda, and K. Ogawa, "Evaluation of received signal power in on-body dynamic channel considering human walking motion," in *2018 Prog. Electromagn. Res. Symp.*, Toyama, Japan, Aug. 2018, pp. 2036–2040.

[17] K. N. Ramli, R. A. Abd-Alhameed, and P. S. Excell, "Interaction of EM fields to the human body using hybrid computational method," *Dev. Complex Electromagn. Probl. using FDTD Subgridding Hybrid Comput. Tech.*, pp. 208–231, 2014.

[18] S. L. Cotton and W. G. Scanlon, "Received signal characteristics of the indoor off-body communications channel at 5.8 GHz," in *2013 IEEE Antennas Propag. Soc. Int. Symp.*, Jul. 2013, pp. 1952–1953.

[19] A. Felaco, K. Y. Kapusuz, H. Rogier, and D. Vande Ginste, "Efficient modeling of on-body passive UHF RFID systems in the radiative near-field," *IEEE Trans. Antennas Propag. [early access].*

[20] C. A. Balanis, *Antenna Theory: Analysis and Design.* John Wiley & Sons, 2015.

[21] J. G. Van Bladel, *Electromagnetic Fields.* John Wiley & Sons, 2007, vol. 19.

[22] B. Wang, D. Chen, B. Zhang, W. Zhang, M. H. Cho, and W. Cai, "Taylor expansion based fast multipole method for 3-D Helmholtz equations in layered media," *J. Comput. Phys.*, vol. 401, no. 16, pp. A3954–A3981, Jan. 2020.

[23] J. A. Stratton, *Electromagnetic Theory.* John Wiley & Sons, 2007, vol. 33.

[24] E. G. Williams, *Fourier Acoustics: Sound Radiation and Nearfield Acoustical Holography.* Academic press, 1999.

[25] C. Cappellin, O. Breinbjerg, and A. Frandsen, "Properties of the transformation from the spherical wave expansion to the plane wave expansion," *Radio Sci.*, vol. 43, no. 1, p. RS1012, Feb. 2008.

[26] W. C. Chew, J.-M. Jin, and E. Michielssen, *Fast and Efficient Algorithms in Computational Electromagnetics.* Artech house, 2001.

[27] J. McKernan, *Hermitian Inner Products.* Massachusetts Institute of Technology, 2008. [Online]. Available: https://bit.ly/3gwRBRV

[28] H. Haber, *The Tensor Spherical Harmonics.* Santa Cruz Institute for Particle Physics, 2017. [Online]. Available: https://bit.ly/3iFikyk

[29] J. Winter, "Tensor spherical harmonics," *Lett. Math. Phys.*, vol. 6, no. 2, pp. 91–96, Mar. 1982.

[30] M. Abramowitz and I. A. Stegun, *Handbook of Mathematical Functions with Formulas, Graphs, and Mathematical Tables.* US Government printing office, 1964, vol. 55.

[31] NSI-MI Technologies. [Online]. Available: https://bit.ly/3cVj7qy

[32] S. Agneessens, "Coupled eighth-mode substrate integrated waveguide antenna: small and wideband with high-body antenna isolation," *IEEE Access*, vol. 6, pp. 1595–1602, 2018.

[33] MATLAB R2019a. [Online]. Available: https://bit.ly/3eQadN4

[34] CST Studio Suite 2019. [Online]. Available: https://bit.ly/3fn96Um

[35] MATLAB R2019a. [Online]. Available: https://bit.ly/3ooK77h

[36] A. I. Sabbah, N. I. Dib, and M. A. Al-Nimr, "SAR and temperature elevation in a multi-layered human head model due to an obliquely incident plane wave," *Prog. Electromagn. Res. M*, vol. 13, pp. 95–108, 2010.